

ELECTRONIC CONTROL OF EDGE-MODE SPECTRUM OF INTEGER-HALL-EFFECT 2D ELECTRON WAVEGUIDES

GUENNADI A. KOUZAEV

*Department of Electronics and Telecommunication, Norwegian University of
Science and Technology-NTNU, Trondheim, No-7491, Norway*

guennadi.kouzaev@iet.ntnu.no

Preprint of an article submitted for consideration in International Journal of
Modern Physics B ©, 12.03.2015, copyright World Scientific Publishing
Company, www.worldscientific.com/worldscinet/ijmpb/

Abstract: In this paper, the control of the edge-mode spectrum of integer-Hall-effect 2D waveguides by electric field is proposed and modeled. Under certain found conditions, the applied transversal electric field allows refining the modal spectrum from non-localized waves, and, additionally, it can switch the edge-mode from the propagating to the evanescent state, and it is interesting in the design of the edge-mode off/on logic components. These waveguides, arbitrary biased by potentials, are described by the Pauli spin-less charge equation and are simulated using the order reduction method of partial differential equations in its Kron's quantum-circuit representation. Additionally to the spectrum control mechanism, the influence of strong-magnitude disorder of chemical potential and magnetic field on the edge localization and modal switching is studied to simulate the arisen-in-practice limitations on these effects.

Keywords: Integer Hall effect; 2D electron waveguide; topological insulator; electronically-controlled edge-mode off/on components

1. Introduction

The goal of this paper is to discover the electronically-controlled mechanism of the edge-mode formation in the integer-Hall-effect 2D waveguides and their off/on switching by electric field in the conditions perturbed by the randomness of potentials.

In general case, the behavior of electron in external electromagnetic (EM) field is described by quantum-mechanical equation [1] proposed by W. Pauli in 1927. A particular case of this equation for a spin-less charge in open space was analytically solved by L. Landau who found the magnetic fields allowing solvable equations [2] and discretization of energy levels of electron in magnetic field. This effect causes quantization of the Hall-transversal resistance of 2D electron waveguides [3], which was discovered in 1980, and it is known today as the *integer quantum* Hall effect because of this resistance is proportional to an integer number of a quantum level [4].

Solutions of full Schrödinger-Pauli equation highlight the *quantum spin* Hall-effect interesting in physics, electronics and quantum computing [5]-[8].

Besides, the integer Hall-effect, the *fractional* one is known to appear in 2D/3D multi-electron waveguides [8]-[10]. In these quantum conductors, the charge carriers interact with each other and with heavy molecules, and many interesting phenomena are known including the edge modes appearing with or without external magnetic field and at low or room temperatures [11]-[13]. All these effects can provide topologically-protected edge mode propagation when some properties of energy surfaces allow the scattering-less charge transportation [12]. Unfortunately, in practice, the modal spectrum of topological insulators is contaminated by non-localized modes, and the edge waves are harmed by parasitic randomness of electric, chemical and magnetic vector potentials. Besides, all possibilities of electronic control of formation of edge modes and their switching by applied electric field have not been discovered in full.

Taking into account that the quantum Hall-effect components can be interesting in practical noise-immune edge-mode logic components and quantum computers, there is a strong need to study in more details the background effects, including the purification of modal spectrum from non-localized waves, the edge-mode switching by electric field, and modeling of the influence of occurring-in-practice randomness of potentials on the modal formation and their switching.

For the sake of simplicity, a 2D integer Hall-effect waveguide is chosen as the study object because of the fundamentality of the modeled modal properties. Following [10]-[12], it is supposed that they are common to more complicate in physics fractional Hall-effect waves formed by electronic clouds.

In Section 2, the waveguide geometries are given. The used algorithm for simulation is considered in Section 3. The results of simulation of waveguides biased by magnetic field are in Section 4, where the influence of strong regular and random disorder of potential and magnetic field on edge localization are modeled and analyzed to highlight the harming effects that may arise in practice. In Section 5, the proposed technique of joint electronic and magnetic purification of the waveguide's spectrum from the non-localized modes is given, and the electronic switching of effect of edge modes is discovered. The conclusions are given in Section 6.

2. Geometry of Studied Electron Waveguides Biased by Magnetic and Electric Fields

A quasi-two-dimensional electron waveguide, in which the control of modal spectrum is modeled in this paper, is shown in Fig. 1. In this waveguide, limited by ideal hard-walls, the forward electron modes are propagating along the axis Oz

and backward ones are against this axis, which is normal to the picture plane in Fig. 1.

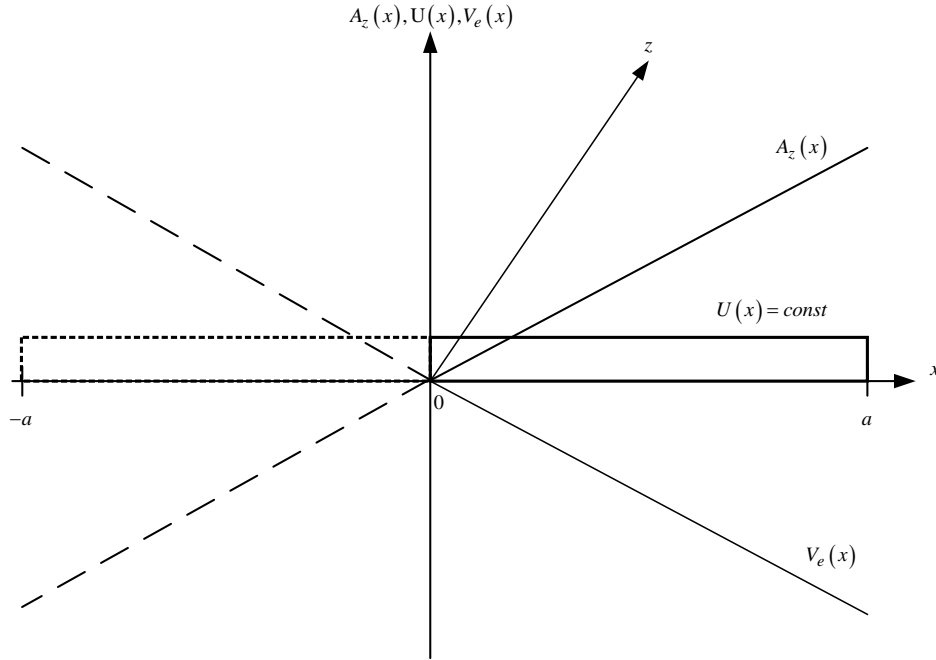


Fig.1. Cross-section of a 2D electron waveguide with the constant potential U and linearly-dependent scalar electric potential $V_e(x)$ and vector magnetic potential component $A_z(x)$. Only right side of the waveguide and the backward-propagating modes are simulated due the symmetry of geometry and applied potentials.

In general, waveguide can be biased by longitudinal vector magnetic potential $A_z = B_0 y$ with B_0 as the magnetic field magnitude and by scalar electric potential $V_e(x) = -eE_0^{(x)}x$, ($e = 1.620218 \cdot 10^{-19}$ C) is the electron charge and $E_0^{(x)}$ is the electric x -oriented field intensity magnitude), and chemical potential $U(x)$ which can be of constant, regular-lattice, or random-lattice shapes.

The non-uniformity of potential $U(x)$ can be caused using different materials in heterostructures, by controlled doping of layers [14], or by injection of carriers to each layer. Additionally, this potential can be influenced by electric field

through the piezoelectric effect [15]. In thin nano-or quasi-2D nano-layers, the effective electron mass m_e as well as the chemical potential U can be controlled electronically [16],[17]. These layers can be staked in piles of height up to several hundreds of micron or even several millimeters, and they can be the best candidates for experimental study of the discovered in this paper effects.

3. Spin-less Charge Schrödinger Equation and its Treatment by Equivalent Circuit Approach

Spin-less charge in magnetic field is described with the reduced Schrödinger-Pauli equation that does not take into account the electron spin:

$$\left[\frac{1}{2m_e} \left(\frac{\hbar}{j} \nabla - e\mathbf{A}(x) \right)^2 + U(x) + V_e(x) - E \right] \psi(x, z) = 0 \quad (1)$$

where $\hbar = 1.05457 \cdot 10^{-34}$ J·s is the normalized Plank constant, $\nabla \equiv \mathbf{x}_0 \frac{\partial}{\partial x} + \mathbf{z}_0 \frac{\partial}{\partial z}$,

$\nabla^2 \equiv \frac{\partial^2}{\partial x^2} + \frac{\partial^2}{\partial z^2}$, \mathbf{x}_0 and \mathbf{z}_0 are the unit vectors, j is imaginary unit, $\mathbf{A}(x)$ is the

magnetic vector potential, E is the electron kinetic energy, $m_e = 0.067m$, and $m = 9.109 \cdot 10^{-31}$ kg .

Supposing that the operator $\left(\frac{\hbar}{j} \nabla - e\mathbf{A}(x) \right)$ is commutative and following to the Landau's guage rule [2], the magnetic vector potential is chosen as $\mathbf{A} = \mathbf{z}_0 B_0 x$. Then $\mathbf{B} = -\nabla \times \mathbf{A}$ has only one $B_y = B_0$ component oriented along the y -axis. Due to the symmetry of Fig. 1's geometry, consider to simulate the right part of waveguide and only backward propagating modes traveling against the z -axis, $\psi(x, z) = \psi(x) e^{-jk_z z}$ (k_z is the modal propagation constant). Equ. (1) is transformed into

$$\left[-\frac{\hbar^2}{2m_e} \frac{d^2}{dx^2} + V(x) - E \right] \psi(x) = 0 \quad (2)$$

where

$$V(x) = \frac{e^2 B_0^2 x^2}{2m_e} + \frac{\hbar e B_0 k_z x}{2m_e} + \frac{\hbar^2 k_z^2}{2m_e} - eE_0^{(x)} x + U(x). \quad (3)$$

As it is seen from (3), $V(x) \sim \mp k_z$ and it defines the direction-depending properties of matter waves. Additionally, the waves depend on the orientation of magnetic and electric fields because $V(x) \sim \pm B_0$ and $V(x) \sim \pm E_0^{(x)}$.

Analytical solution of equ. (2) is considered in [2],[5] for infinite plane with $U(x)=0$ and $E_0^{(x)}=0$, and where the wavefunctions are found as the Hermite polynomials multiplied by exponents. A numerical model for a 2D electron waveguide of a limited width and for zero potential and electric field is given in [5],[7].

Below, a more general theory is given for calculation of an electron waveguide controlled by magnetic, electric and chemical potentials. This theory is based on the method of the order reduction of the Schrödinger equation proposed in [18] and elaborated further for many applications, including the multilayered electron waveguide models and cold matter nonlinear Schrödinger equation simulation [19]-[23].

Following these approaches, equ. (2) is transformed into a system of the first-order differential equations regarding to the equivalent quantum “voltage” $u(x) = \psi(x)$ and “current” $i(x) = j \frac{\hbar}{m_e} \frac{du(x)}{dx}$ for general $V(x)$:

$$\begin{aligned} \frac{du(x)}{dx} &= -j \frac{m_e}{\hbar} i(x), \\ \frac{di(x)}{dx} &= \frac{2j}{\hbar} (V(x) - E) u(x) \end{aligned} \quad (4)$$

Implementing equ. (4) by boundary condition $u(x=0,a)=0$, we obtain the boundary value problem, which solution gives us the propagation constant k_z and modal wavefunction $\psi(x)e^{-jk_z z}$ for any backward-propagating (z -axis) modes. In a similar manner, the forward-propagating (z -axis) modes are treated.

Consider the x -dependence, equ. (4) is the Kirchhoff’s law for the voltage $u(x)$ and current $i(x)$ at any point of this axis. Suppose that this axis is divided into a number K of domains Δx_k where the potential $V(x_k) = \text{const}$ (Fig. 2). Then, these domains can be considered as the short lengths of a transversal

transmission line, which have their own propagation constants $k_x^{(k)}$ and characteristic impedances $Z_c^{(k)}$ and described by their transfer matrices $A^{(k)}$ (see for more details [23]):

$$A^{(k)} = \begin{pmatrix} \cos k_x^{(k)} \Delta x_k & jZ_c^{(k)} \sin k_x^{(k)} \Delta x_k \\ \frac{j}{Z_c^{(k)}} \sin k_x^{(k)} \Delta x_k & \cos k_x^{(k)} \Delta x_k \end{pmatrix}. \quad (5)$$

Here, $k_x^{(k)} = \sqrt{\frac{2m_e}{\hbar^2} (V(x_k) - E)}$, and $Z_c^{(k)} = \frac{\sqrt{m_e}}{\hbar k_x^{(k)}}$.

Next step in this algorithm is choosing an arbitrary reference point X_0 (Fig. 2) at which the left \tilde{Z} and right \bar{Z} impedances are obtained using multiplication of corresponding matrices A_k .

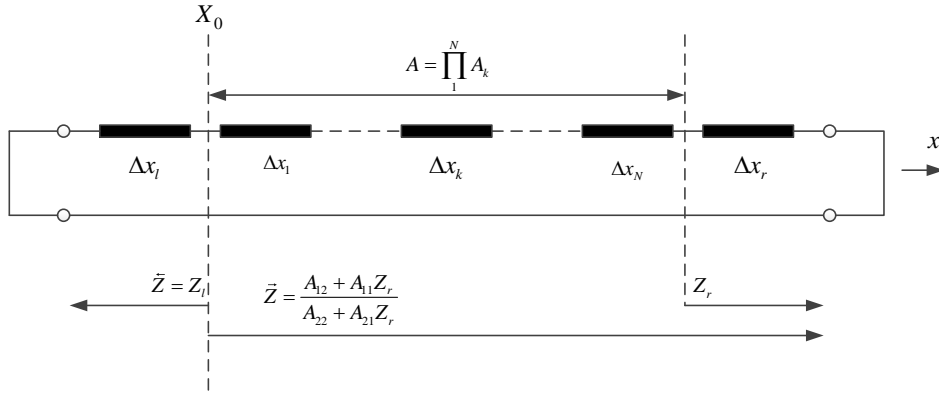


Fig. 2. Transversal transmission line model for 2D electron waveguide. The left- and right-side shortenings correspond to the hard walls of this waveguide at $x=0, a$, correspondingly.

To find the longitudinal propagation constant k_z , the condition of the transversal resonance is written at $x = X_0$ (Fig. 2):

$$\tilde{Z} + \bar{Z} = 0. \quad (6)$$

It gives a nonlinear and transcendental equation regarding to k_z . To calculate the voltage and current distributions along the x -axis, its source is placed at the reference point X_0 and their amplitudes are obtained using an iteration scheme from [24]:

$$\begin{pmatrix} u_k \\ i_k \end{pmatrix} = A_k \begin{pmatrix} u_{k+1} \\ i_{k+1} \end{pmatrix}. \quad (7)$$

This algorithm requires inversion of matrices A_k , which is performed here analytically. Proper normalization of these matrices allow to avoid or essentially decrease the instability [23], which is typical for most calculations with the transfer matrices. Additionally, the voltage or wavefunction is normalized as

$$\int_0^a u(x) \frac{1}{m_e} u^*(x) dx = 1 \quad (8)$$

where the star sign (*) means the conjugation operation over complex, in general, $u(x) = \psi(x)$.

4. Transversal Disorder of Potential and the Edge-mode Formation

There are many contributions on the study of disordered conductors and semiconductors and on the influence of magnetic field on their conductivity [5]. The randomness in them is considered as the technologically-caused small-magnitude imperfections. Particularly, it has been shown how the Integer-Hall effect suppresses the influence of these imperfections. The 2D electron waveguides can be formed by stacking the semiconductor few-nanometer layers or even 2D atom planes, and their chemical potential may vary in the few-electron-volt range [14]-[16] and even strong localization of the Anderson type can appear in such stacks. These disorders can shift the Hall localization towards stronger magnetic fields which is an unwanted effect. Besides, the biasing magnetic field on the nano-level may show its granularity, and this effect destroys the localization according to known experiments. Below, some simulations are shown for large-magnitude chemical and magnetic potential transversal disorders.

Our simulations start with a waveguide which chemical potential $U(x) = const$ as a reference structure. This potential was chosen at the level $U(x)/E = U_0/E = 0.8667$ with electron energy $E = 0.1$ eV. For magnetic field $B_0 = 0$, the propagation constant k_z was compared with the analytically calculated value $k_z = \sqrt{\frac{2m_e}{\hbar^2}(E - U_0) - \left(\frac{\pi}{a}\right)^2}$, and no difference was found for six meaningful digits after the period sign (Fig. 3).

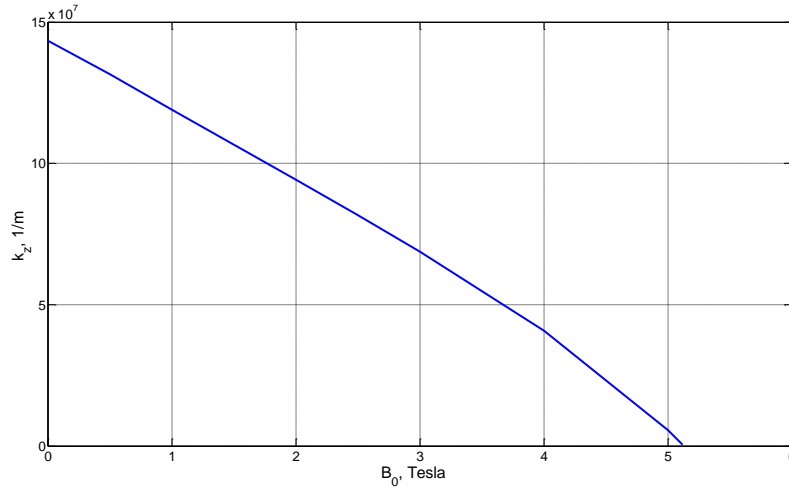


Fig. 3. Dependence of the main-mode propagation constant k_z versus magnetic field B_0 .
 $U_0/E=0.8667$ and $a=58.5$ nm.

The squared wavefunction has no difference with the corresponding function of homogeneous 2D electron waveguide (Fig. 4, solid-blue line). The overall number of domains is hold $K=1060$ that supports practically complete convergence of results in most calculations performed for the waveguide's width $a=58.5$ nm [23].

To study the effect of magnetic field, it increases gradually, and a set of calculations of propagation constant and squared wavefunction $|\psi|^2$ of only main mode was performed here because for the given waveguide geometry, particle energy, and potential, the higher-order modes are evanescent, i.e. they are not propagating. The propagation constant dependence (Fig. 3) was calculated for $B_0=0-5.12$ T, and it tends to zero with magnetic field. More dramatic changes are in the mode's wavefunction (Fig. 4).

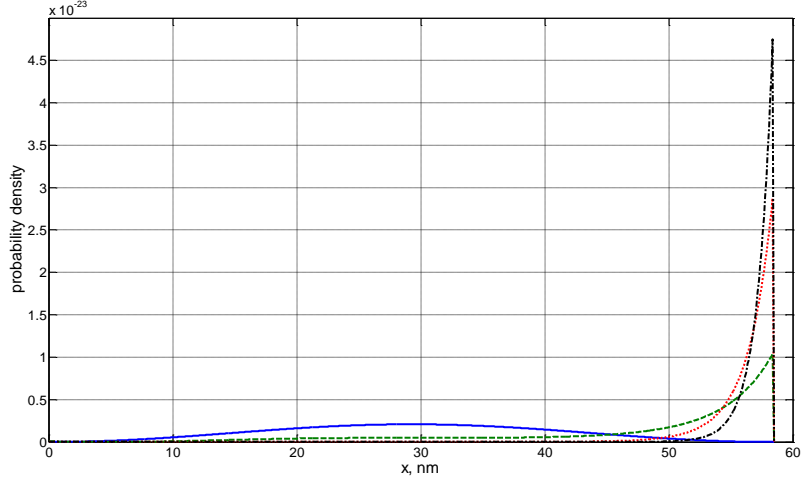


Fig. 4. Probability-density shapes in regular potential electron waveguide. $U_0/E=0.8667$ and $a=58.5$ nm. Blue-solid line: $B_0=0$ T ; green-dash line: $B_0=1.5$ T ; red-dot line: $B_0=3$ T ; black dot-dash line: $B_0=5.12$ T .

Its evolution starts with $\sim \sin^2\left(\frac{\pi x}{a}\right)$ for $B_0=0$. According to theory of Hall-effect in 2D electron waveguides, the main mode of this waveguide is localized with B_0 , and it is transformed into the edge-type mode which pick is “pressed” to the right side of waveguide due to wave’s backward type. Due to the properly chosen geometry, potential, and electron energy, this waveguide is monomodal, and electron transportation by this edge mode can be realized without contamination of this process by non-localized waves, which was found harmful in many cases. The first transversally-disordered waveguide studied here is formed using the *regular-lattice potential* $U_{\text{lattice}}(x)$ (Figs. 1b, 5), and it was generated according to the following formula [23]:

$$U_{\text{lattice}}(x) = U_0 \cdot \text{rem}(N, 2) \quad (9)$$

where U_0 is the magnitude coefficient, and $\text{rem}(2, N)$ is the Matlab reminder-after-division function.

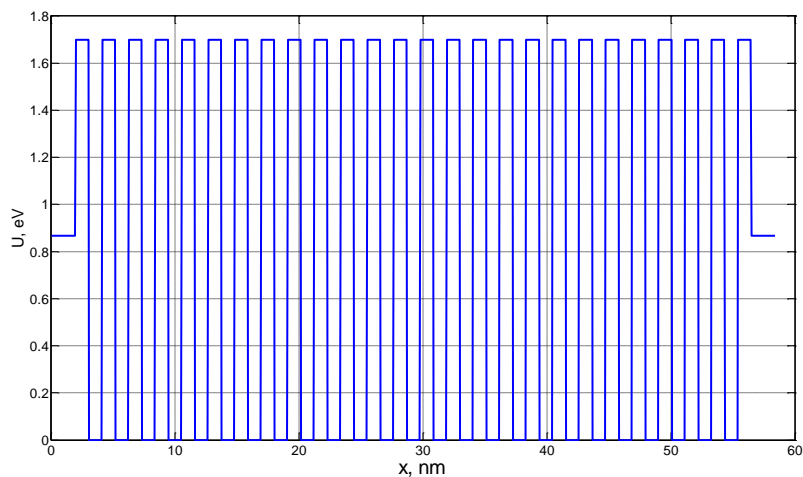


Fig. 5. Regular-lattice potential $U_{\text{lattice}}(x)$ with $U_0/E=1.7$ given for a 2D-waveguide. Other waveguide parameters: $a=58.5$ nm and $N=51$. Additional left and right potential steps given for $\Delta x_l = 2$ nm and $\Delta x_r = 2$ nm (see Fig. 2) are on the level $0.5U_0$.

With the magnetic-field increase from $B_0 = 0$ to 6 T, the longitudinal propagation constant k_z decreases (Fig. 6).

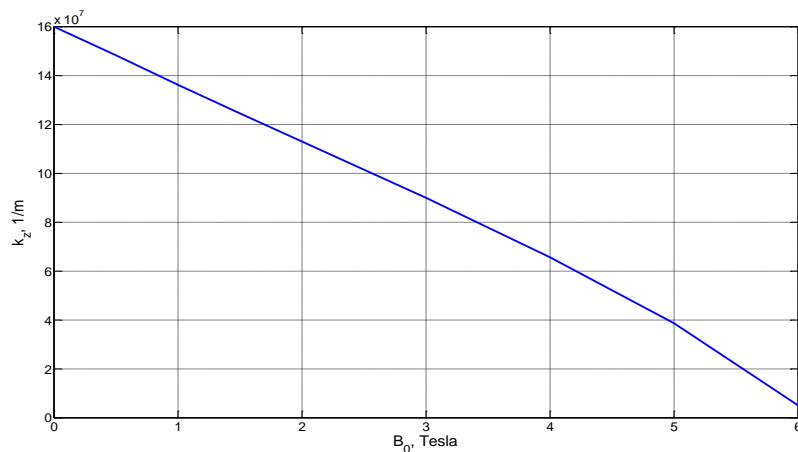


Fig. 6. Propagation constant k_z dependence versus magnetic field B_0 in regular lattice-potential waveguide. $U_0/E=1.7$, $a=58.5$ nm, and $N=51$.

A set of probability-density plots corresponding to these simulations are in Fig. 7.

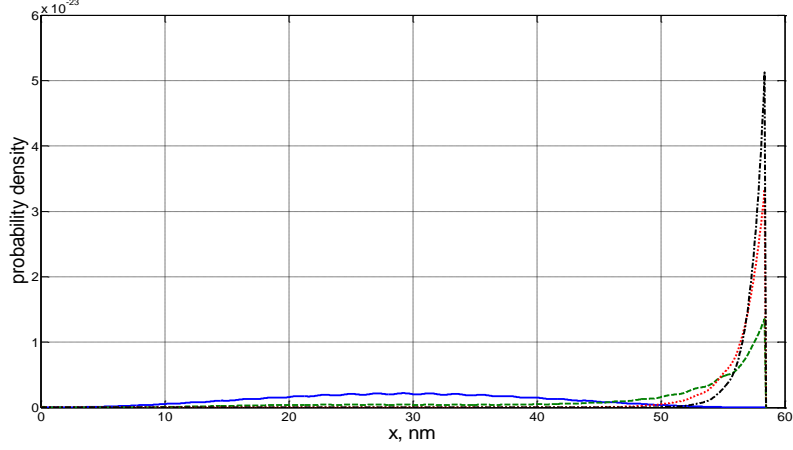


Fig. 7. Probability-density shapes in regular lattice potential electron waveguide. $U_0/E=1.7$, $N=51$, and $a=58.5$ nm. Blue-solid line: $B_0=0$ T; green-dash line: $B_0=1.5$ T; red-dot line: $B_0=3$ T; black dot-dash line: $B_0=5$ T.

It is seen that this lattice-shaped potential ($U_0/E=1.7$) prevents from the edge-mode formation. It occurs at stronger magnetic field B_0 in comparison with the constant-potential waveguide (Figs. 1a, 3, 4). Additional effect of this lattice is that this waveguide starts to be multimodal for the same geometry and electron energy as in the case of Fig. 1a due to lower averaged potential.

Pseudo-random lattice potential waveguides can form the localized modes if their lattice step Δx_k is comparable with $\lambda/2\pi = \hbar/\sqrt{2m_e E}$. This effect is found in many optical, microwave and acoustic waveguides which media is randomly perturbed [25],[26].

Following [23], the pseudo-random potential $U_{\text{random}}(x)$ (Fig. 8) is generated as

$$U_{\text{random}}(x) = U_0 \cdot \text{rem}(N, 2) A(N). \quad (10)$$

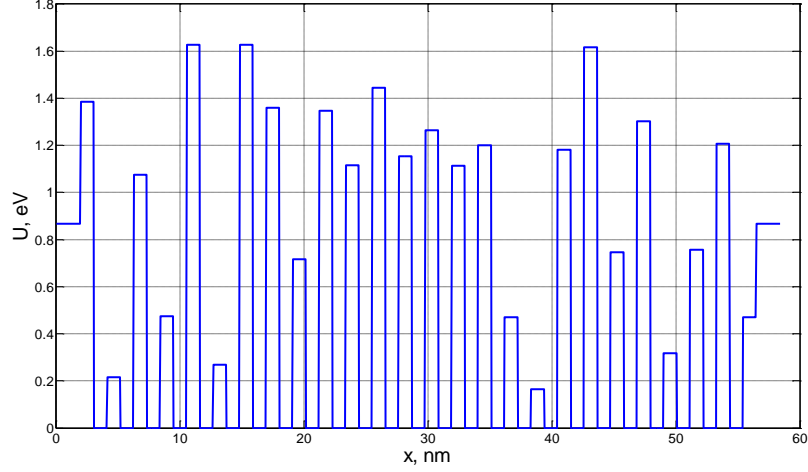


Fig. 8. Pseudo-random lattice potential $U_{\text{random}}(x)$ with $U_0/E=1.7$. Waveguide parameters: $a=58.5$ nm and $N=51$. Additional left and right potential steps for $\Delta x_l=2$ nm and $\Delta x_r=2$ nm (see Fig. 2) are chosen on the level of the averaged value of this pseudo-random potential.

where $A(N)$ is N -sample pseudo-random data obtained using the Matlab's *rand.m* function in its default regime in this case.

In [23], the formation of localized modes is studied in pseudo-random lattice potential, and it is noticed on the combined mechanism formation of localized modes in these waveguides. The randomness and reflections from the ideal “hard” walls form some localized shapes, which are found relative stable towards variation of random potential sets.

One of the modal shapes corresponding to the potential shown in Fig. 8 and formed in this waveguide is in Fig. 9 (blue-solid line). It is formed at the right waveguide's side if $B_0=0$. The extremum of this curve may be connected with the local lacunas of this random potential (Fig. 8), and it is rather unstable with variation of this potential, as it was shown in [23]. This localization is easily destroyed with increase of magnetic field up to 6 T, and the sharp edge-mode shape is after $B_0 > 2-2.5$ T (red-dash and black dash-dot lines). As in the above-described cases, the modal propagation constant decreases monotonically with magnetic field.

One of the findings in [23] (Fig. 7) is the localized by pseudo-random potential main modes which sharp pick shifted to the one side of waveguide. They are formed, mostly, in waveguides with the large width potential steps $\Delta x_k > \hbar/\sqrt{2m_e E}$ (Fig. 10).

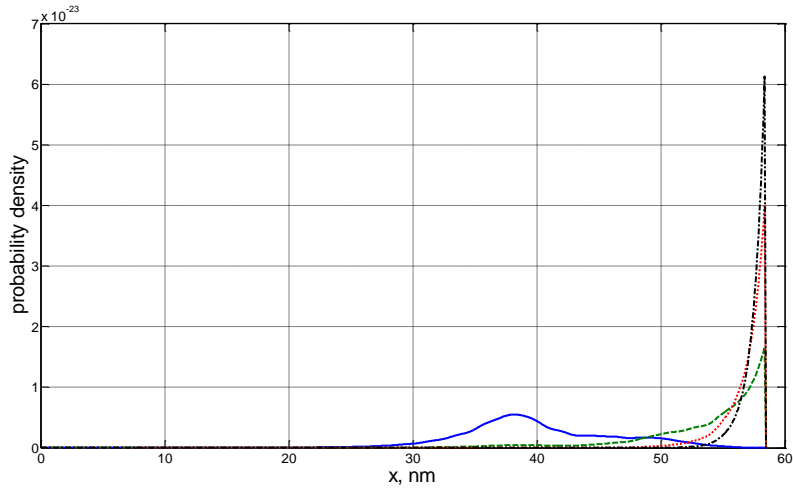


Fig. 9. Probability-density shapes in pseudo-random lattice potential (Fig. 8) electron waveguide. $U_0/E=1.7$ and $a=58.5$ nm. Blue-solid line: $B_0=0$ T ; green-dash line: $B_0=1.5$ T ; red-dot line: $B_0=3$ T ; black dot-dash line: $B_0=5$ T .

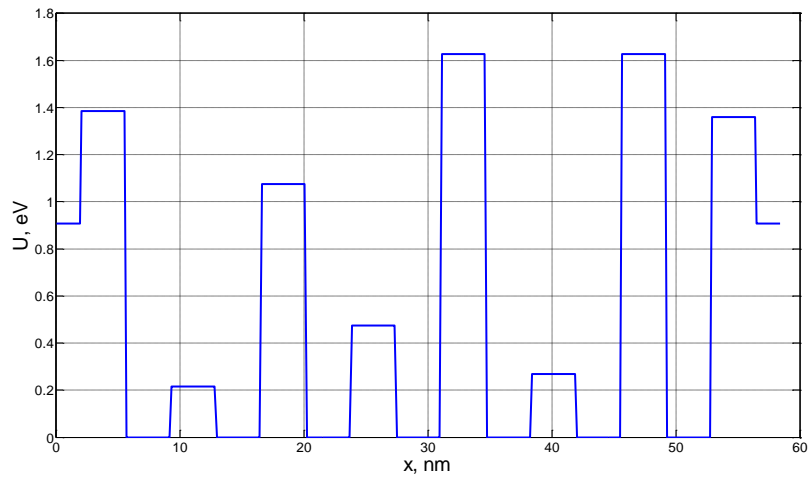


Fig. 10. Pseudo-random lattice potential $U_{\text{random}}(x)$ with $U_0/E=1.7$. Waveguide parameters: $a=58.5$ nm, and $N=15$. Additional left and right potential steps given for $\Delta x_l=2$ nm and $\Delta x_r=2$ nm (see Fig. 2) are chosen on the level of the averaged value of this pseudo-random potential.

These modal shapes (Fig. 11, blue-solid line) are rather stable being the products of interference of reflected partial transversal waves from the ideal hard walls at $x=0, a$ and from random-potential steps. It is seen from this picture, that the non-biased by magnetic field pseudo-random potential waveguides can deliver the same shapes (Fig. 11, blue-solid line) as those in magnetic field (Fig. 11, black-dash line).

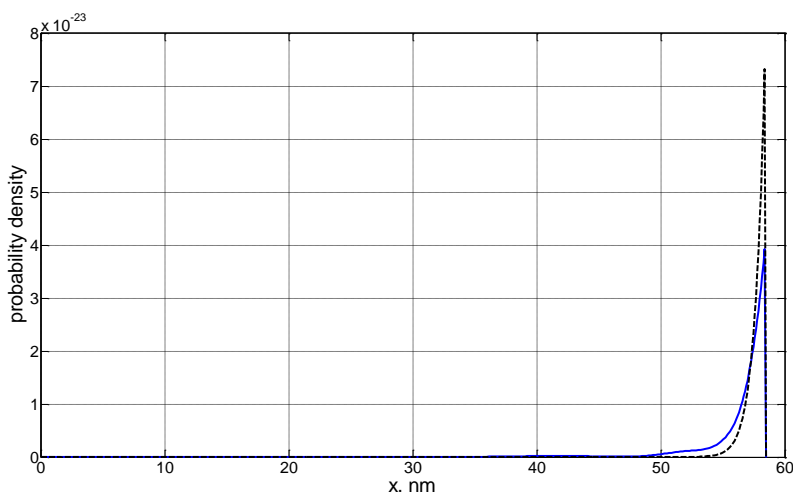


Fig. 11. Probability-density shapes in pseudo-random lattice potential (Fig. 10) electron waveguide. $U_0/E=1.7$, $\Delta x_l = \Delta x_r = 2$ nm, (see Fig. 2) and $a=58.5$ nm. Blue-solid line: $B_0=0$ T and black-dash line: $B_0=5$ T.

It is interesting how these two mechanisms of formation of localized shapes are working together. In this purpose, it has been performed statistical study of stability of the pick shapes taking into account the random content of the potential $V(x)$. We generated 15 sets of pseudo-random potential with $U_0/E=1.7$ and $N=15$ using the default and shuffle regimes of the Matlab's *rand.m* function. The left and right potentials from Fig. 10 are kept on the averaged level of the generated lattice.

For each of the three values of magnetic field ($B_0 = 0, 1, 3$ T), we performed 15 calculations of wavefunction. It was found that stability of the mentioned pick shape was growing with the magnetic field. For instance, at $B_0 = 0$ and 1 T, only 8 shots (from 15) preserved the sharp pick. At $B = 3$ T, already 14 shots (from 15) gave the localized wavefunctions. Here, the randomness of chemical potential

$U(x)$ plays a perturbative role, and these picks can be even sharper with the combination of random potential and magnetic field instead of separate biasing by these fields.

It is interesting to study the influence of *randomness of magnetic field*. It may occur due to magnetic clusters of molecules randomly distributed in some materials [27]. There, it was found experimentally that the edge-mode formation due to the fractional spin quantum Hall effect was destroyed in many cases. Although we model the integer quantum Hall effect, this may take a place in our case, too. Unfortunately, equ.1 is handled further here only if magnetic field is constant in the x -direction because of the requirements to satisfy the Landau gauge condition. To keep this requirement, we suppose that the magnetic field is constant in the limits of each domain Δx_k only. But the value of magnetic field $B_0^{(k)}$ can be varied randomly from k -th domain to another (Fig. 12). It is calculated according to the following formula

$$B_0^{(k)} = B_0(1 - \alpha A(k)) \quad (11)$$

where $A(k)$ is from the pseudo-random set $A(N)$ generated using the Matlab's *rand.m* function in its default state, and the parameter $0 < \alpha < 1$ defines the randomness magnitude.

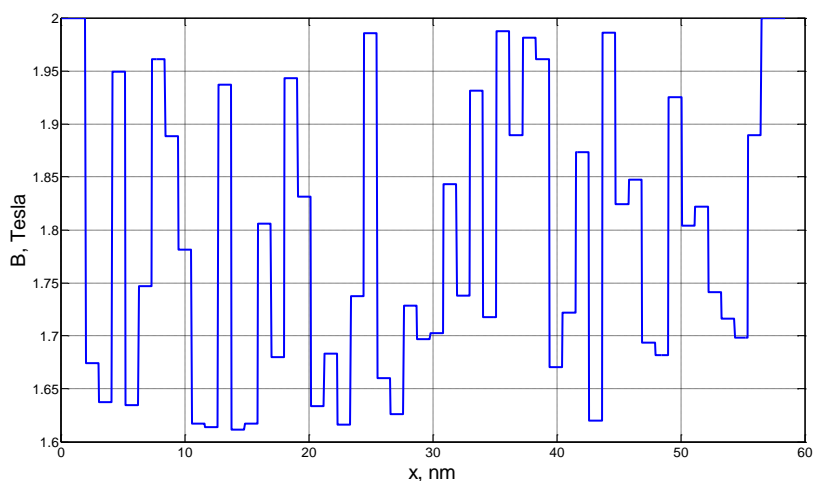


Fig. 12. Pseudo-random magnetic field magnitude $B_0^{(k)}$ generated according to (11). $\alpha = 0.2$, $B_0 = 2$ T, $a = 58.5$ nm, $\Delta x_l = \Delta x_r = 2$ nm, and $N = 51$.

Some simulation results are shown in Fig. 13.

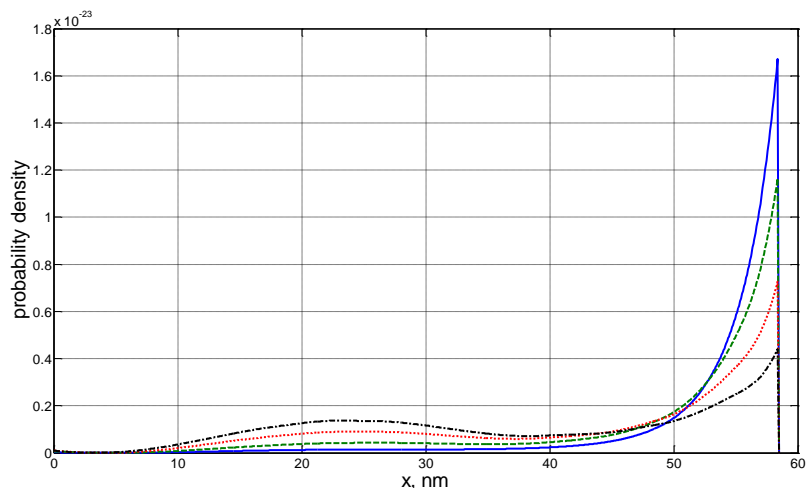


Fig. 13. Probability-density shapes in electron waveguide biased by pseudo-random magnetic field (Fig. 12) and constant potential $U_0/E=0.8867$. Blue-solid line: $\alpha=0.1$, green-dash line: $\alpha=0.5$; red-dot line: $\alpha=0.8$; black dot-dash line: $\alpha=1$. $B_0=2$ T, $a=58.5$ nm, and $N=51$.

It is seen that the essential delocalization of wavefunction starts for $\alpha=0.5-0.6$. In general, they are in accordance with the experiments [27] on harmful influence of random magnetic clusters on the fractional spin quantum Hall effect.

5. Control of Edge Modes with Electric Field

In general, the Hall-effect waveguides are very polluted by non-localized waves which makes hard using only edge modes for electron transportation. A great interest is in suppressing these non-localized waves and in electronic switching devices for edge modes [28]-[31]. Here, some analogies with the EM waves can be used. Many results are in microwaves where modes are filtered or switched according their spatial topologically-stable content using passive and semiconductor components [22].

Consider Fig. 4, where the probability density in a monomodal waveguide is shown. Unfortunately, this one-mode transportation has its own drawback because of its poor signal-to-noise ratio, and the signaling by multiple edge modes is preferable [28]. Additional freedom in material and in control of its chemical potential allows partly to solve this problem. Choosing an appropriate combination of electron energy, potential and geometry of waveguide, it is made multimodal.

Fig. 14 shows the propagation constant k_z dependence on biasing magnetic field B_0 for the found three propagating modes.

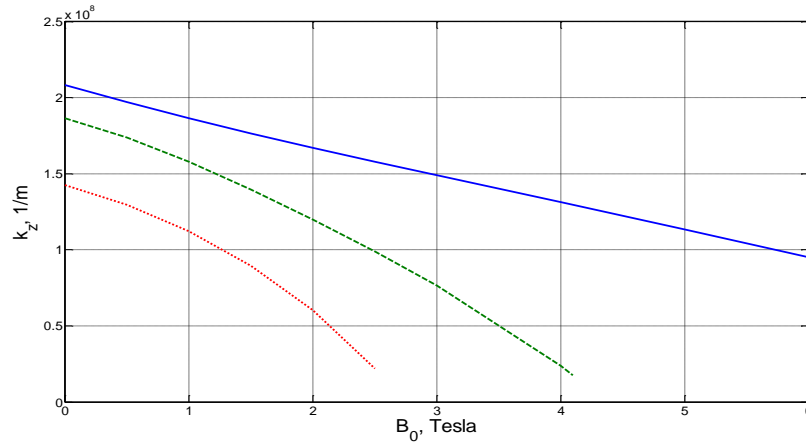


Fig. 14. Propagation constants k_z of the first three modes versus magnetic field B_0 . $U_0/E=0.7367$ and $a=58.5$ nm. Main mode: blue-solid line; 2nd mode: green-dash line; 3rd mode: red-dot line.

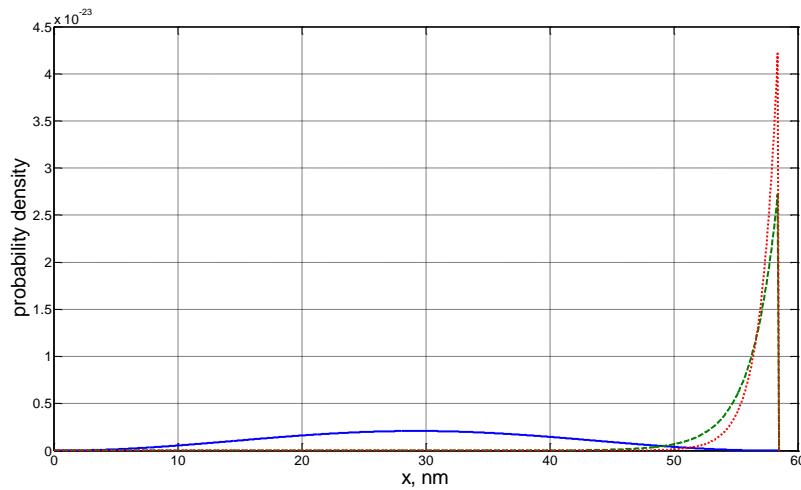


Fig. 15. Probability-density shapes of main mode in constant-potential. Blue-solid line: $U_0/E=0.7367$ and $a=58.5$ nm. Blue-solid line: $B_0=0$ T; green-dash line: $B_0=2.5$ T; red-dot line: $B_0=4$ T.

The mentioned potential is of 85% of that for the monomodal waveguide (Figs. 3, 4), in this case. Simulation of wavefunctions with the magnetic-field increase

shows that localization starts with the main mode (Fig. 15), and it is following with the second one (Fig. 16).

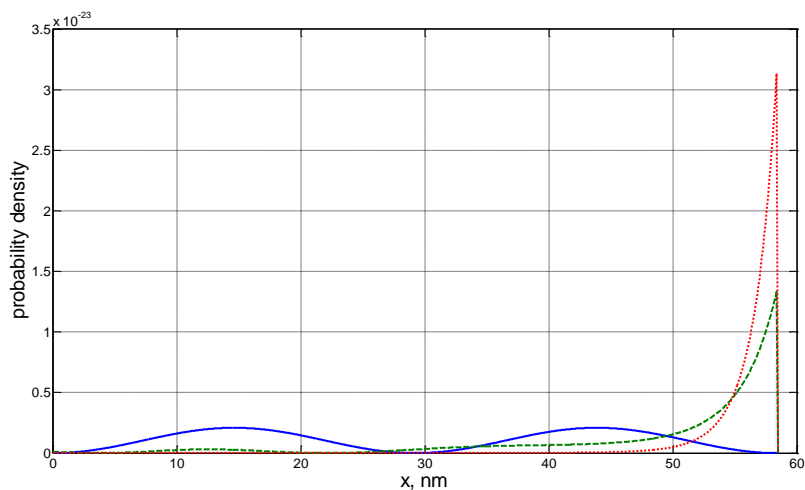


Fig. 16. Probability-density shapes of the 2nd mode in constant-potential. $U_0/E=0.7367$ and $a=58.5$ nm. Blue-solid line: $B_0=0$ T ; green-dash line: $B_0=2.5$ T ; red-dot line: $B_0=4$ T .

The third mode is coming to be non-propagating in its non-localized state in this waveguide at $B_0=5.2$ T . (Fig. 17).

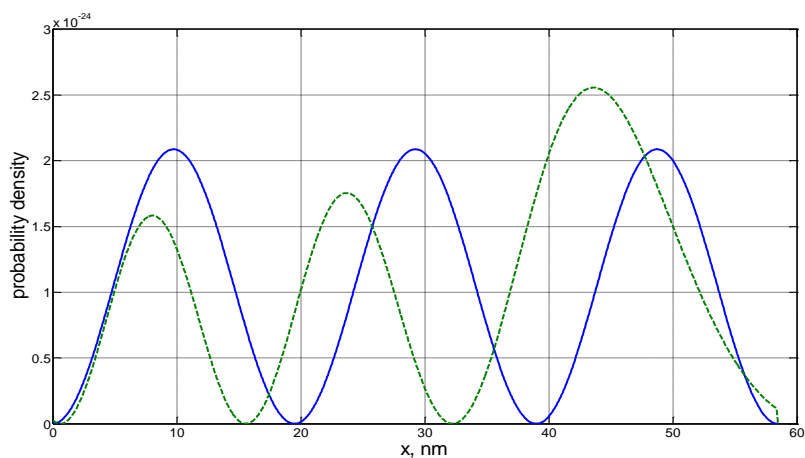


Fig. 17. Probability-density shapes of the 3rd mode in constant-potential electron waveguide. $U_0/E=0.7367$ and $a=58.5$ nm. Blue-solid line: $B_0=0$ T ; green-dash line: $B_0=2.5$ T .

Then, for magnetic field over $B_0 \geq 5.2$ T , *electron transportation can be realized by only two edge-localized modes.*

Although there are several mechanisms how to vary the chemical potential electronically, the edge-mode transportation can be controlled by the applied in the x -direction electric field without changing the potential $U(x)$ (see equ. 1). For instance, Fig. 18 shows evolution of wavefunction with electric field $E_0^{(x)}$ increase.

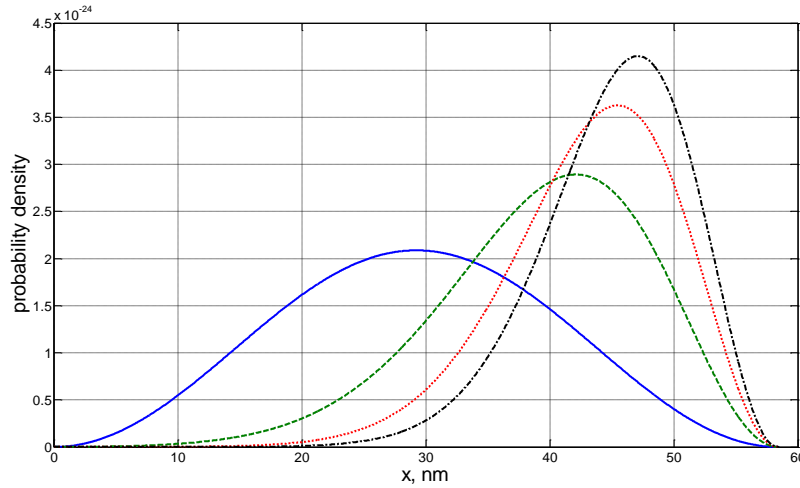


Fig. 18. Probability-density shapes in electron waveguide biased by electric field $E_0^{(x)}$. $B_0 = 0$ T , $U_0/E = 0.8667$, and $a = 58.5$ nm . Blue-solid line: $E_0^{(x)} = 0$ V/m ; green-dash line: $E_0^{(x)} = 3 \cdot 10^5$ V/m ; red-dot line: $E_0^{(x)} = 6 \cdot 10^5$ V/m ; black dot-dash line: $E_0^{(x)} = 9 \cdot 10^5$ V/m .

It is seen that electron tends to the side with lower potential (see equ. (3)), and the wavefunction is localized slightly at the right part of waveguide. The propagation constant increases with electric field, and it can be used for electronic control of propagation characteristics of modes.

Applying strong electric field to waveguides biased by weak magnetic field leads to destruction of edge localization caused by opposite signs of terms with the magnetic and electric fields in (3), and it is seen from Fig. 19, *where electric field transforms localized shape (solid line) into a main mode shape deformed by electric field (dot-dash line).*

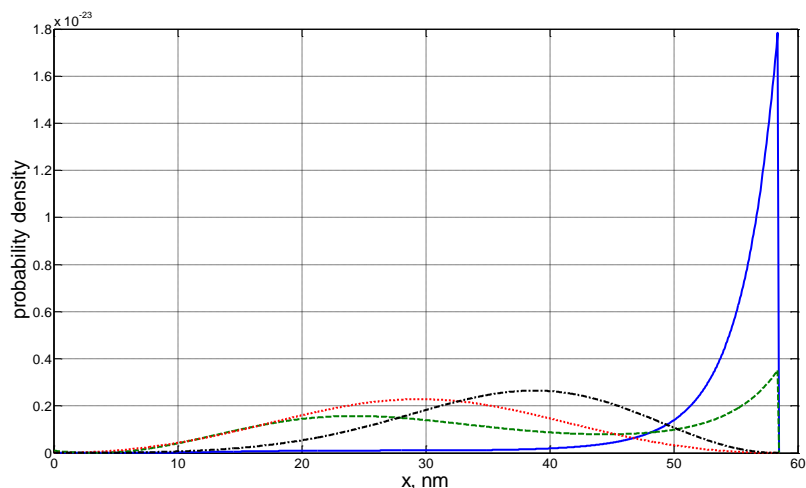


Fig. 19. Probability-density shapes in electron waveguide biased by electric field $E_0^{(x)}$. $B_0 = 2$ T, $U_0/E = 0.8667$, and $a = 58.5$ nm. Blue-solid line: $E_0^{(x)} = 0$ V/m; green-dash line: $E_0^{(x)} = 3 \cdot 10^5$ V/m; red-dot line: $E_0^{(x)} = 6 \cdot 10^5$ V/m; black dot-dash line: $E_0^{(x)} = 9 \cdot 10^5$ V/m.

Then, this effect is similar to that found in [28] where a multilayer structure allows to transform the edge modes to non-localized ones by application of vertical-to-sandwich electric field. Both components (from [28] and our simple structure) can be considered as the intermodal switches.

It is interesting to notice that varying the electric field, an intermediate basic shape is found (Fig. 19, red-dot line) which is similar to the one for waveguide biased only by constant chemical potential (Fig. 4, blue-solid line). The electric field value providing this shape can be considered as a critical one that corresponds in our case approximately $E_0^{(x)} = 6 \cdot 10^5$ V/m. Lower electric fields provide the localized modal shapes (Fig. 19, solid-blue and green-dot lines). Stronger electric field gives the waveforms of this basic shape distorted by electric field (Fig. 19, black dot-dash line).

The electronic components based on the different mode signaling relate to the active-pause devices [22] because in their non-edge state, the signal (de-localized mode) is still at the output of a circuit. The best switches and signals are with the passive pause when in the off-state no energy appears at the output of a device. It decreases the energy consumption and increases the signal-to-noise ratio.

By simulation, it is found that a combination of proper chosen magnetic and electric fields allows to *switch electronically the edge-localized mode from its*

evanescent to the propagating condition and back in a simple way. In this purpose, consider Fig. 3, where the main mode becoming evanescent near $B_0 = 5.2$ T. Fig. 20 (blue-solid line) shows increase of real propagation constant from its zero value with the applied electric field $E_0^{(x)}$ given for strong magnetic field $B_0 = 5.5$ T.

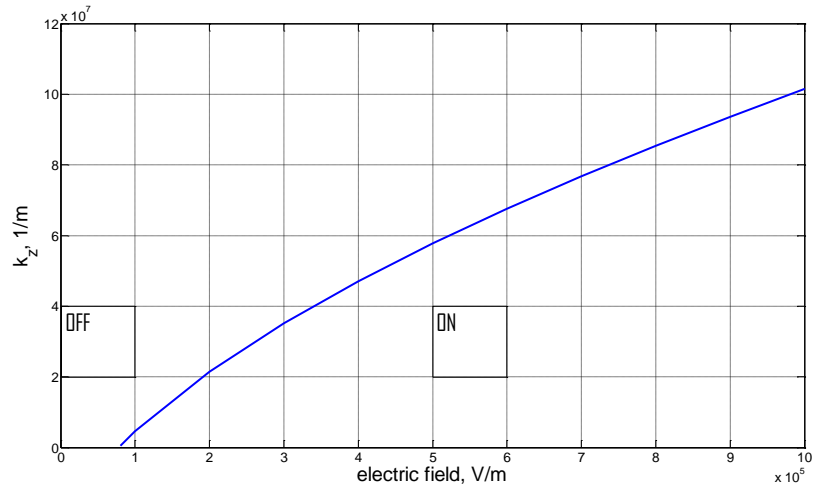


Fig. 20. Propagation constant k_z of the edge-localized main mode versus electric field $E_0^{(x)}$. $U_0/E = 0.8667$, $B_0 = 5.5$ T, and $a = 58.5$ nm.

Thus, if $0 < E_0^{(x)} < 0.8 \cdot 10^5$ V/m, the main mode is not propagating, and the signal appears at the end of waveguide only due to tunneling effect that can be chosen negligible enough by lengthening of waveguide or by increasing magnetic field.

For $E_0^{(x)} > 0.8 \cdot 10^5$ V/m, a large signal, which is transported by propagating main mode, is at the end of waveguide length. For this wide range of electric field values $0.8 \cdot 10^5 < E_0^{(x)} < 10^6$ V/m and for the chosen magnetic field $B_0 = 5.5$ T, the electric field does not harm the edge-localized shape of main mode (Fig. 21) and this waveguide with its properly chosen parameters can work in switching regime, which is illustrated in Table. 1.

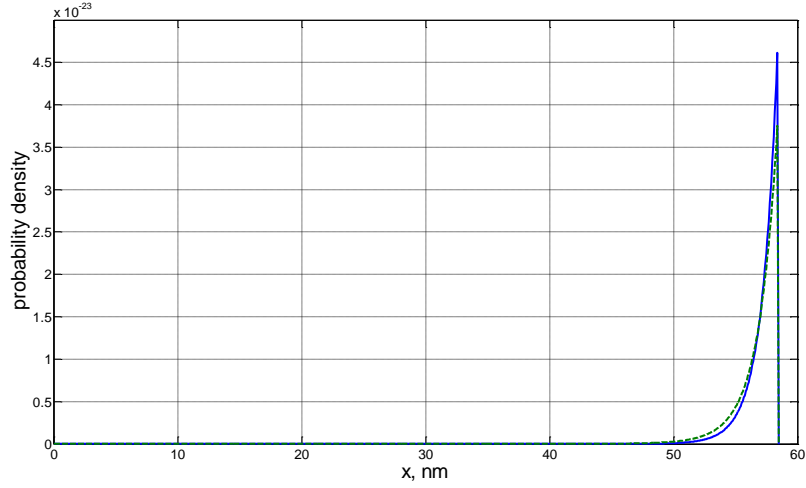


Fig. 21. Probability-density shapes in electron waveguide biased by electric field $E_0^{(x)}$. $B_0 = 5.5$ T, $U_0/E = 0.8667$, and $a = 58.5$ nm. Blue-solid line: $E_0^{(x)} = 2 \cdot 10^5$ V/m; green-dash line: $E_0^{(x)} = 10^6$ V/m.

Table. 1. Truth-table of proposed waveguide switch of edge modes

L	Control electric field $E_0^{(x)}$ level	Output logical state
1	$0 < E_0^{(x)} < 0.8 \cdot 10^5$ V/m	0
2	$0.8 \cdot 10^5$ V/m $< E_0^{(x)} < 10^6$ V/m	1

To estimate the parameters of this switch connected to the source and load, it is necessary to calculate the device currents in the *on* and *off* regimes. For this purpose, similarly to [5], the Landauer-Buttiker formalism can be used.

6. Results and Conclusions

It has been shown how the modal spectrum of the integer-Hall effect 2D waveguide can be controlled by applied transversal electric field, including the refining of the waveguide's spectrum from the propagating non-localized waves and switching of the rest traveling edge modes to their evanescent state and back. All these discovered effects are interesting in the development of new quantum coherent edge-mode logic components. The mentioned waveguides and the effects in them have been studied using the partial differential equation order reduction method in its Kron's circuit interpretation allowing semi-analytical modeling of waveguides arbitrary-biased by the chemical, magnetic and electric potentials. The effect of the potential randomness influencing the electronic modal spectrum control has been studied in details, which is interesting from the practical design point of view.

7. References

- [1]. W. Pauli, *Zeitschrift für Physik* **43**, 601 (1927).
- [2]. L. D. Landau and E. M. Lifschitz, *Quantum Mechanics: Non-relativistic Theory. Course of Theoretical Physics. Vol. 3* (Pergamon Press, London, 1977).
- [3]. K. von Klitzing, G. Dorda, and M. Pepper, *Phys. Rev. Lett.* **45**, 494 (1980).
- [4]. D. J. Thouless, M. Kohomoto, M. P. Nightingale, *et al.*, *Phys. Rev. Lett.* **49**, 405 (1982).
- [5]. D. K. Ferry, S. M. Goodnik, and J. Bird, *Transport in Nanostructures* (Cambridge Univer. Press, Cambridge, 2009).
- [6]. S. Bandyopadhyay and M. Cahay, *Introduction to Spintronics* (CRC Press, US, 2008).
- [7]. D. Venturelli, V. Giovannetti, F. Tadei *et al.*, *Phys. Rev. B* **83**, 075315 (2011).
- [8]. X. -L. Qi and S. -C. Zhang, *Phys. Today* **63**, 33 (2010).
- [9]. D. C. Tsui, H. L. Stormer, and A. C. Gossard, *Phys. Rev. Lett.* **48**, 1559 (1982).
- [10]. R. B. Laughlin, *Phys. Rev. Lett.* **50**, 1395 (1983).
- [11]. C. L. Kane and M. P. A. Fisher, *Edge-state Transport*, Chpt. 4, pp. 109-159, In: *Perspectives in Quantum Hall Effects*. Eds. S. D. Sarma and A. Pinczuk (John Wiley & Sons, Inc., US, 1997).
- [12]. M.Z. Hasan and C. L. Kane, *Rev. Mod. Phys.* **82**, 3045 (2010).
- [13]. J.W. Linder, *Physics* **3**, 66 (2010).
- [14]. P. V. Balachandran and J. M. Rondinelli, *Nat. Commun.* **6**, 6191 (2015).
- [15]. G. Rijnders and D. H. A. Blank, *Nature* **433**, 369 (2005).
- [16]. S. Z. Butler, S. M. Hollen, L. Cao *et al.*, *ACS Nano* **7**, 2898 (2013).

- [17]. G. Fiori, F. Bonaccorso, G. Innaccone *et al.*, *Nat. Nanotechn.* **9**, 768 (2014).
- [18]. G. Kron, *J. Appl. Phys.* **16**, 172 (1945).
- [19]. H. Sanada, M. Suzuki, and N. Nagai, *IEEE J. Q. Electron.* **33**, 731 (1997).
- [20]. R. Kaji and M. Koshiba, *IEEE J. Q. Electron.* **31**, 8 (1995).
- [21]. R. Kaji and M. Koshiba, *IEEE J. Q. Electron.* **30**, 1971 (1994).
- [22]. G. A. Kouzaev, *Applications of Advanced Electromagnetics. Components and Systems* (Springer-Verlag, Berlin-Heidelberg, 2013).
- [23]. G. A. Kouzaev, *Int. J. Mod. Phys.* **28**, 1350192 (2014).
- [24]. G. Zelinger, *Basic Matrix Analysis and Synthesis* (Pergamon Press, New York, 1966).
- [25]. D. S. Wiersma, *Nat. Photonics* **7**, 188 (2013).
- [26]. P. Hsieh, C. Chung, J. F. McMillan *et al.*, *Nat. Phys.*, published online February 2, 2015.
- [27]. I. Lee, C. K. Kim, J. Lee *et al.*, *PNAS* **112**, 1316 (2015).
- [28]. X. Qian, J. Liu, and J. Li, *Science* **346**, 1344 (2014).
- [29]. R. Mellnik, J. S. Lee, A. Richardella *et al.*, *Nature* **511**, 449 (2014).
- [30]. L. Chirulli, D. Venturelli, F. Taddei *et al.*, *Phys. Rev. B* **85**, 155317 (2012).
- [31]. A. Endo, N. Shibata, and Y. Iye, *Physica E* **42**, 1042 (2010).